UDC 621. 396

BOUNDARY PROBLEM SOLUTION FOR EIGENMODES IN COAXIAL QUAD-RIDGED WAVEGUIDES

Fedir F. Dubrovka, Stepan I. Piltyay

National Technical University of Ukraine “Kyiv Polytechnic Institute”, Kyiv, Ukraine

The boundary problem for eigenmodes in coaxial quad-ridged waveguides has been solved by the transverse field-matching technique. The formulas obtained provide possibilities to calculate cutoff wave numbers and electric and magnetic fields distributions of TEM, TE and TM modes in the presence of the ridges either on the inner or on the outer perfectly conducting cylinder. The analysis of the dependences of cutoff wave numbers and electric field distributions convergences on the number of partial modes has been carried out. It has been shown that for calculation of cutoff wave numbers with residual error less than 0.1 % it is enough to utilize 27 partial modes, and for the correct calculation of fields distributions one should utilize more than 30 partial modes.

Introduction

Ridged structures are widely used in modern waveguide devices. The utilization of ridges enables to create ultrawideband devices, to provide ultrawideband matching of hollow waveguides with coaxial transmission lines and to create discontinuities of required type in narrowband devices. Ridged structures are used in filters [1–3], polarizers [4–6], waveguides [7–10], antennas [11–13], orthomode transducers [14–16], lasers [17–19], resonators [20, 21] and other devices.

For development of the devices based on ridged structures one needs to know modal characteristics of ridged waveguides, namely, eigenmodes cutoff frequencies (or cutoff wave numbers) and their fields distributions. The characteristics of ridged waveguides' eigenmodes for rectangular cross-section have been analyzed in [22–24]. The eigenmodes of square ridged waveguides have been investigated in [9]. The eigenmodes of ridged waveguides for circular cross section have been analyzed in [24]. The eigenmodes of elliptical ridged waveguides have been investigated in [10]. The eigenmodes of rectangular coaxial ridged waveguides have been analyzed in [8]. In [25] authors of this paper have solved the boundary problem for sectoral coaxial ridged waveguides using integral equation technique, and in [26] their eigenmodes have been analyzed.

In this paper the boundary problem solution for the coaxial quad-ridged waveguides (CQRW) has been obtained using transverse field-matching technique and the solutions convergence analysis has been performed for the dependences of cutoff wave numbers and electric field distributions (EFD) on the number of partial modes.

Problem statement

Configurations of hollow infinite CQRW under study and denotations of their cross sectional dimensions are shown in Fig. 1, namely, the CQRW with ridges on the inner perfectly conducting cylinder is depicted in Fig. 1*a*, and the CQRW with ridges on the outer cylinder is shown in Fig. 1*b* (hereinafter referred to as subscripts "in" and "out" respectively).

We will investigate only that eigenmodes, for which the CQRW vertical symmetry plane ($\phi = 0$) is a magnetic wall. Due to the symmetry of the CQRW relative to the horizontal plane $\phi = \pi / 2$, it is expedient to obtain the boundary problem solution separately for the eigenmodes with antisymmetric and symmetric relative to that plane EFD. Consequently, the fields distributions in the region III will be, respectively, antisymmetric or symmetric relative to the distributions in the region I. The eigenmodes with symmetric relative to the plane $\phi = \pi / 2$ EFD can be conventionally divided into two types: 1) the eigenmodes with symmetric EFD relative to the plane $\varphi = \pi / 4$, 2) the eigenmodes with antisymmetric EFD relative to the plane $\varphi = \pi / 4$. For the eigenmodes with antisymmetric EFD the plane $\varphi = \pi / 2$ is the electric wall, and for the eigenmodes with symmetric EFD it is the magnetic wall. Besides, for the eigenmodes with symmetric EFD relative to the plane $\varphi = \pi / 2$, that are also antisymmetric relative to the plane $\varphi = \pi / 4$, that plane is electric wall, for the eigenmodes, EFD of which are symmetric relative to the plane $\varphi = \pi / 4$, it is magnetic wall.

Consequently, for the TE and the TM eigenmodes with antisymmetric EFD the boundary problem should be solved only for the region limited by the magnetic wall $\phi = 0$, by the electric wall $\varphi = \pi / 2$ and by perfectly conducting circular cylinders with radii $r = a$, $r = b$ (see Fig.

2). For the eigenmodes with symmetric EFD relative to the plane $\varphi = \pi/2$ the boundary problem should be solved only for the region limited by the magnetic wall $\phi = 0$, and by electric or by magnetic wall $\phi = \pi/4$ (for the eigenmodes, respectively, with antisymmetric or symmetric EFD relative to it) and by perfectly conducting circular cylinders with radii $r = a$, $r = b$ (see Fig. 3).

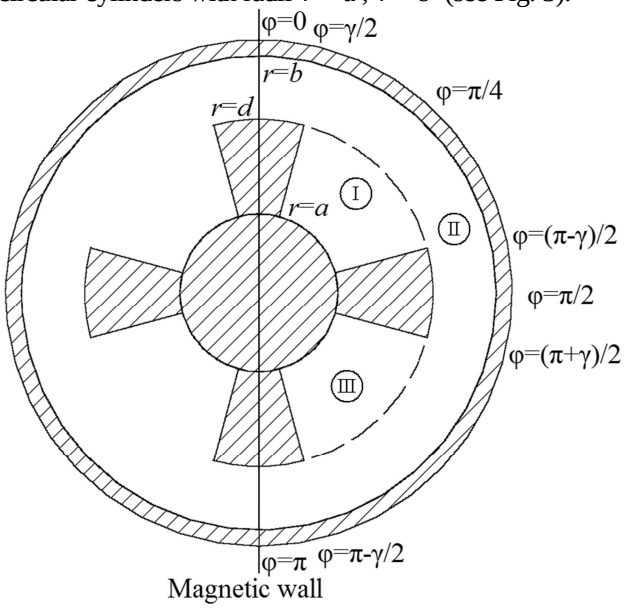

(*a*)

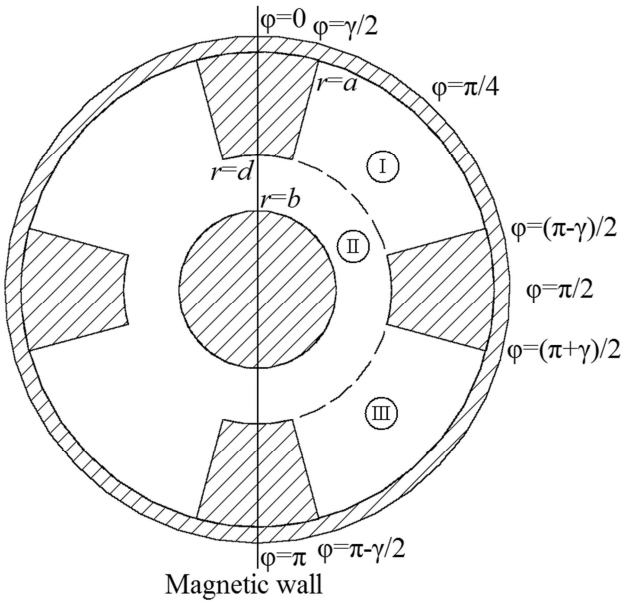

(*b*)

Fig. 1. Cross sections of coaxial quad-ridged waveguides with ridges: (*a*) on inner conducting circular cylinder; (*b*) on outer conducting circular cylinder.

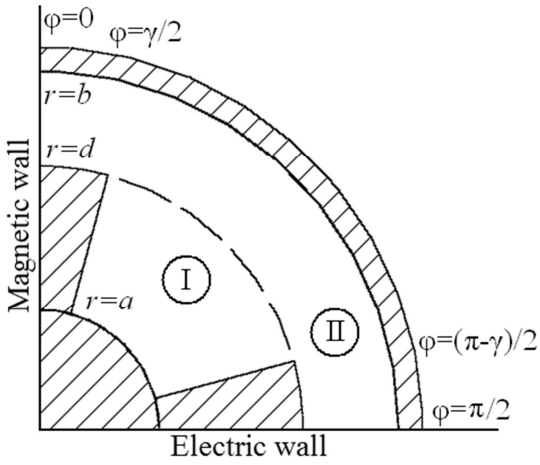

(*a*)

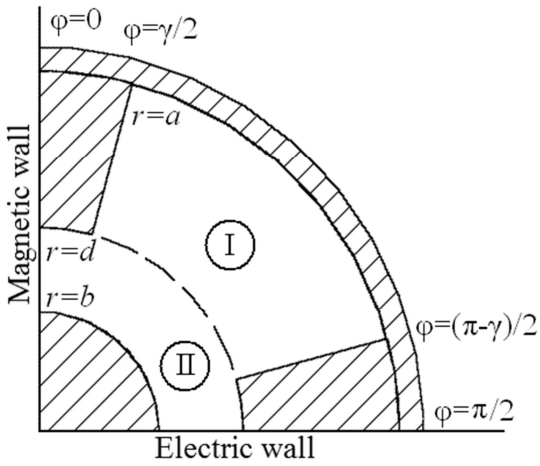

(*b*)

Fig. 2. Computational models of coaxial quad-ridged waveguides with ridges: (*a*) on inner conducting circular cylinder; (*b*) on outer conducting circular cylinder.

EFD of the TEM mode are symmetric relative to not only the planes $\phi = 0$ and $\phi = \pi/2$, but also relative to the planes $\phi = \pi/4$ and $\phi = 3\pi/4$, because all four ridges have the same potential. Therefore for the TEM mode the CQRW has four magnetic walls ($\phi = 0$; $\pi/4$; $\pi/2$; $3\pi/4$). Consequently, for the analysis of TEM eigenmode it is necessary to solve boundary problem only for the region limited by the magnetic walls $\phi = 0$, $\phi = \pi/4$ and by perfectly conducting circular cylinders with radii $r = a$, $r = b$ (see Fig. 3, in which both walls should be chosen as magnetic ones).

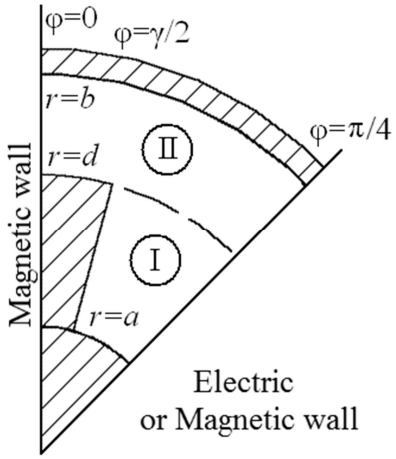

(*a*)

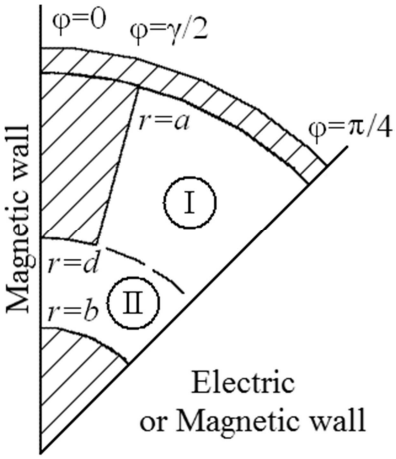

(*b*)

Fig. 3. Computational models of coaxial quad-ridged waveguides taking into account symmetry properties with ridges: (*a*) on inner conducting circular cylinder; (*b*) on outer conducting circular cylinder.

TEM eigenmode

In the regions I and II (Fig. 3, in which both walls should be chosen as magnetic ones) we represent the electric field components E_r and E_ϕ in the form of infinite sums of the partial modes with unknown amplitudes, each of which satisfies the Maxwell equations in the cylindrical coordinate system and boundary conditions at the magnetic walls and at the perfectly conducting surfaces of CQRW:

$$E_r^{\mathrm{I}}(r,\phi)=\sum_{n=0}^{\infty}A_n\sin[l_1(n)(\phi-\gamma/2)]r^{-1+l_1(n)}\,; \qquad (1)$$

$$E_r^{\mathrm{II}}(r,\phi)=\sum_{m=0}^{\infty}B_m\cos[l_2(m)\phi]r^{-1-l_2(m)}\,; \qquad (2)$$

$$E_\phi^{\mathrm{I}}(r,\phi)=\sum_{n=0}^{\infty}A_n\cos[l_1(n)(\phi-\gamma/2)]r^{-1+l_1(n)}\,; \qquad (3)$$

$$E_\phi^{\mathrm{II}}(r,\phi)=\sum_{m=0}^{\infty}B_m\sin[l_2(m)\phi]r^{-1-l_2(m)}\,, \qquad (4)$$

where $l_1(n)=2\pi(2n+1)/(\pi-2\gamma)$; $l_2(m)=4m$; A_n, B_m are unknown amplitude coefficients.

The boundary conditions at the interface between the regions I and II (Fig. 3) are as follows:

$$E_r^{\mathrm{II}}(r=d,\ \phi\in[\gamma/2;\ \pi/4])=$$
$$=E_r^{\mathrm{I}}(r=d,\ \phi\in[\gamma/2;\ \pi/4])\,; \qquad (5)$$

$$E_\phi^{\mathrm{II}}(r=d,\ \phi\in[\gamma/2;\ \pi/4])=$$
$$=E_\phi^{\mathrm{I}}(r=d,\ \phi\in[\gamma/2;\ \pi/4])\,. \qquad (6)$$

Besides, at the perfectly conducting surface of the ridge at $r=d$ and $\phi\in[0;\ \gamma/2]$:

$$E_\phi^{\mathrm{II}}(r=d,\ \phi\in[0;\ \gamma/2])=0\,. \qquad (7)$$

Having substituted (1)–(4) in (5)–(7), we obtain:

$$\sum_{m=0}^{\infty}B_m\cos[l_2(m)\phi]d^{-1-l_2(m)}=$$
$$\sum_{n=0}^{\infty}A_n\sin[l_1(n)(\phi-\gamma/2)]d^{-1+l_1(n)}\,,\ \phi\in[\gamma/2;\ \pi/4]\,; \qquad (8)$$

$$\sum_{m=0}^{\infty}B_m\sin[l_2(m)\phi]d^{-1-l_2(m)}=$$
$$\sum_{n=0}^{\infty}A_n\cos[l_1(n)(\phi-\gamma/2)]d^{-1+l_1(n)}\,,\ \phi\in[\gamma/2;\ \pi/4]\,, \qquad (9)$$

$$\sum_{m=0}^{\infty}B_m\sin[l_2(m)\phi]d^{-1-l_2(m)}=0\,,\ \phi\in[0;\ \gamma/2]\,. \qquad (10)$$

Multiplying left and right parts of the equation (8) by the system of functions $\sin[l_1(p)(\phi-\gamma/2)]$, $p=0,1,2,...$ and integrating the resulting relation at the interval $[\gamma/2;\ \pi/4]$, at which the system of these functions is orthogonal, we obtain

$$\sum_{m=0}^{\infty}B_mI_1(p,m)d^{-1-l_2(m)}=A_p\frac{\pi-2\gamma}{8}d^{-1+l_1(p)}\,, \qquad (11)$$

from whence it follows, that the amplitude of the p-th partial mode in the region I (Fig. 3)

$$A_p=8\sum_{m=0}^{\infty}B_mI_1(p,m)d^{-1-l_2(m)}/[(\pi-2\gamma)d^{-1+l_1(p)}]\,. \qquad (12)$$

The value of $I_1(p,m)$ in the formulas (11), (12) is determined by the relation

$$I_1(p,m)=\int_{\gamma/2}^{\pi/4}\cos[l_2(m)\phi]\sin[l_1(p)(\phi-\gamma/2)]\mathrm{d}\phi .$$

In the same way, the amplitude of the p-th partial mode in the region I (Fig. 3) can be derived from (9) as

$$A_p=8\sum_{m=0}^{\infty}B_m I_2(p,m)d^{-1-l_2(m)}/[(\pi-2\gamma)d^{-1+l_1(p)}], \quad (13)$$

where $I_2(p,m)=\int_{\gamma/2}^{\pi/4}\sin[l_2(m)\phi]\cos[l_1(p)(\phi-\gamma/2)]\mathrm{d}\phi$.

Having equated (12) and (13), we obtain the system of equations

$$\sum_{m=0}^{\infty}B_m I_1(p,m)d^{-1-l_2(m)}=\sum_{m=0}^{\infty}B_m I_2(p,m)d^{-1-l_2(m)};$$

$$\sum_{m=0}^{\infty}B_m d^{-1-l_2(m)}\left[I_1(p,m)-I_2(p,m)\right]=0 . \quad (14)$$

Simplifying the expressions (14) yields the result

$$\sum_{m=0}^{\infty}B_m F_1(p,m)=0,\ p=0,1,2,..., \quad (15)$$

where $F_1(p,m)=d^{-1-l_2(m)}\left[I_1(p,m)-I_2(p,m)\right]$.

Next, we multiply left and right parts of the equation (10) by the system of functions $\sin[l_2(q)\phi]$, $q=0,1,2,...$ and integrate the obtained relation at the interval $[0;\ \gamma/2]$. As a result, we get

$$\sum_{m=0}^{\infty}B_m I_3(q,m)d^{-1-l_2(m)}=0, \quad (16)$$

where $I_3(q,m)=\int_{0}^{\gamma/2}\sin[l_2(m)\phi]\sin[l_2(q)\phi]\mathrm{d}\phi$.

Simplifying the expression (16) yields the following result:

$$\sum_{m=0}^{\infty}B_m F_2(q,m)=0,\ q=0,1,2,... \quad (17)$$

where $F_2(q,m)=I_3(q,m)d^{-1-l_2(m)}$.

Combining the systems of equations (15), (17) and limiting the number of partial modes in the region II, we obtain the following homogeneous system of linear algebraic equations (SLAE) with unknown partial modes amplitudes B_m:

$$\begin{cases}\sum_{m=0}^{M-1}B_m F_1(p,m)=0, & p=0,1,...,(P-1)\\ \sum_{m=0}^{M-1}B_m F_2(q,m)=0, & q=0,1,...,(M-P-1)\end{cases} . \quad (18)$$

At the fixed number of partial modes M, we define the number of equations of the first type by the angular widths ratio of the regions I and II (Fig. 3) [27] as $P=\mathrm{int}\left[(\pi-2\gamma)M/\pi\right]$, where integer part is rounded up or down.

The system of linear algebraic equations (18) can be rewritten in the matrix form:

$$\begin{bmatrix}F_{0,0} & \cdots & F_{0,M-1}\\ \vdots & \ddots & \vdots\\ F_{M-1,0} & \cdots & F_{M-1,M-1}\end{bmatrix}\begin{bmatrix}B_0\\ \vdots\\ B_{M-1}\end{bmatrix}=\begin{bmatrix}0\\ \vdots\\ 0\end{bmatrix} \quad (19)$$

The elements of the matrix $[F]$ are determined by the following relation

$$F(i,j)=\begin{cases}F_1(i,j), & i=0,1,...,(P-1)\\ F_2((i-P),j), & i=P,\ (P+1),...,(M-1)\end{cases} .$$

The condition of nontrivial solution of the homogeneous SLAE (19) is the equality to zero of the matrix $[F]$ determinant. This condition is satisfied, because the row of the matrix $[F]$ determinant with the index P is zero:

$$F(P,j)=F_2(0,j)=I_3(0,j)d^{-1-l_2(j)}=$$

$$=\int_{0}^{\gamma/2}\sin(4j\phi)\sin(0)\mathrm{d}\phi\cdot d^{-1-l_2(j)}=0 .$$

While solving the homogeneous SLAE (19), the row with the index P must be excluded from the matrix $[F]$.

To solve the homogeneous SLAE (19), let us assume that $B_0=1$. Then, we get:

$$\begin{bmatrix}F_{0,1} & \cdots & F_{0,M-1}\\ \vdots & \ddots & \vdots\\ F_{P-1,1} & \cdots & F_{P-1,M-1}\\ F_{P+1,1} & \cdots & F_{P+1,M-1}\\ \vdots & \ddots & \vdots\\ F_{M-1,1} & \cdots & F_{M-1,M-1}\end{bmatrix}\begin{bmatrix}B_1\\ \vdots\\ B_{M-1}\end{bmatrix}=-\begin{bmatrix}F_{0,0}\\ \vdots\\ F_{P-1,0}\\ F_{P+1,0}\\ \vdots\\ F_{M-1,0}\end{bmatrix};$$

$$\begin{bmatrix} B_1 \\ \vdots \\ B_{M-1} \end{bmatrix} = -\begin{bmatrix} F_{0,1} & \cdots & F_{0,M-1} \\ \vdots & \ddots & \vdots \\ F_{P-1,1} & \cdots & F_{P-1,M-1} \\ F_{P+1,1} & \cdots & F_{P+1,M-1} \\ \vdots & \ddots & \vdots \\ F_{M-1,1} & \cdots & F_{M-1,M-1} \end{bmatrix}^{-1} \begin{bmatrix} F_{0,0} \\ \vdots \\ F_{P-1,0} \\ F_{P+1,0} \\ \vdots \\ F_{M-1,0} \end{bmatrix}.$$

By using these systems of equations, we define all partial mode amplitudes B_m. Then, the partial mode amplitudes A_p are determined by formulas (12) or (13). Further, we find distributions of electric field components in regions I and II (Fig. 3) by the formulas (1)–(4). Electric field components in the whole cross section of CQRW are determined using the EFD symmetry properties of TEM mode. The components of the TEM mode magnetic field can be defined by the formulas: $H_\phi(r,\phi) = E_r(r,\phi)/Z$, $H_r(r,\phi) = -E_\phi(r,\phi)/Z$, where $Z = \sqrt{\mu_a/\varepsilon_a}$ is the mode impedance depending on the CQRW homogeneous filling parameters μ_a, ε_a only.

TE modes antisymmetric relative to the plane $\varphi = \pi/2$

The TE eigenmodes designations introduced in this section coincide with the ones given above for the TEM mode, but they refer only to the TE modes. In the regions I and II (Fig. 2) we represent the fields H_z and E_φ in the form of infinite sums of the partial modes with unknown amplitudes and cutoff wave numbers, each of which satisfies the Maxwell equations in the cylindrical coordinate system and boundary conditions at the magnetic, electric walls and at the perfectly conducting surfaces of CQRW (see Fig. 2):

$$H_z^{\mathrm{I}}(r,\phi) = \sum_{n=0}^{\infty} A_n \cos[l_1(n)(\phi-\gamma/2)]\times$$
$$\times[J'_{l_1(n)}(k_c a)Y_{l_1(n)}(k_c r) - Y'_{l_1(n)}(k_c a)J_{l_1(n)}(k_c r)]; \quad (20)$$

$$H_z^{\mathrm{II}}(r,\phi) = \sum_{m=0}^{\infty} B_m \sin[l_2(m)\phi]\times$$
$$\times[J'_{l_2(m)}(k_c b)Y_{l_2(m)}(k_c r) - Y'_{l_2(m)}(k_c b)J_{l_2(m)}(k_c r)]; \quad (21)$$

$$E_\phi^{\mathrm{I}}(r,\phi) = Z(f,k_{\mathrm{кр}})\sum_{n=0}^{\infty} A_n \cos[l_1(n)(\phi-\gamma/2)]\times$$
$$\times[J'_{l_1(n)}(k_c a)Y'_{l_1(n)}(k_c r) - Y'_{l_1(n)}(k_c a)J'_{l_1(n)}(k_c r)]; \quad (22)$$

$$E_\phi^{\mathrm{II}}(r,\phi) = Z(f,k_{\mathrm{кр}})\sum_{m=0}^{\infty} B_m \sin[l_2(m)\phi]\times$$
$$\times[J'_{l_2(m)}(k_c b)Y'_{l_2(m)}(k_c r) - Y'_{l_2(m)}(k_c b)J'_{l_2(m)}(k_c r)], \quad (23)$$

where $l_1(n) = 2\pi n/(\pi-2\gamma)$; $l_2(m) = 2m+1$; $Z(f,k_c) = 2\pi i f\mu_a/k_c$; A_n, B_m are unknown amplitude coefficients; $J_l(x)$, $Y_l(x)$, $J'_l(x)$, $Y'_l(x)$ are Bessel functions of the first and the second kinds and their derivatives; k_c defines a cutoff mode number; i denotes an imaginary unit; f designates the frequency; μ_a is absolute permeability of CQRW inner medium.

The boundary conditions at the interface between the regions I and II (Fig. 2) are as follows:

$$E_\phi^{\mathrm{II}}(r=d,\ \phi\in[\gamma/2;\ (\pi-\gamma)/2]) =$$
$$= E_\phi^{\mathrm{I}}(r=d,\ \phi\in[\gamma/2;\ (\pi-\gamma)/2]), \quad (24)$$

$$H_z^{\mathrm{II}}(r=d,\ \phi\in[\gamma/2;\ (\pi-\gamma)/2]) =$$
$$= H_z^{\mathrm{I}}(r=d,\ \phi\in[\gamma/2;\ (\pi-\gamma)/2]). \quad (25)$$

On the perfectly conducting surfaces of the ridges at $r=d$ and $\phi\in[0;\ \gamma/2]\cup[(\pi-\gamma)/2;\ \pi/2]$, the following condition is met:

$$E_\phi^{\mathrm{II}}(r=d,\ \phi\in[0;\ \gamma/2]\cup[(\pi-\gamma)/2;\ \pi/2]) = 0 \quad . \quad (26)$$

Having substituted (20)–(23) in (24)–(26), we obtain:

$$\sum_{m=0}^{\infty} B_m \sin[l_2(m)\phi]J'Y'[l_2(m),k_c b,k_c d] =$$
$$= \sum_{n=0}^{\infty} A_n \cos[l_1(n)(\phi-\gamma/2)]J'Y'[l_1(n),k_c a,k_c d],$$
$$\phi\in[\gamma/2;\ (\pi-\gamma)/2]; \quad (27)$$

$$\sum_{m=0}^{\infty} B_m \sin[l_2(m)\phi]J'Y[l_2(m),k_c b,k_c d] =$$
$$= \sum_{n=0}^{\infty} A_n \cos[l_1(n)(\phi-\gamma/2)]J'Y[l_1(n),k_c a,k_c d],$$
$$\phi\in[\gamma/2;\ (\pi-\gamma)/2]; \quad (28)$$

$$\sum_{m=0}^{\infty} B_m \sin[l_2(m)\phi]J'Y'[l_2(m),k_c b,k_c d] = 0,$$
$$\phi\in[0;\ \gamma/2]\cup[(\pi-\gamma)/2;\ \pi/2], \quad (29)$$

where $J'Y(l,x,y) = J'_l(x)Y_l(y) - Y'_l(x)J_l(y)$, $J'Y'(l,x,y) = J'_l(x)Y'_l(y) - Y'_l(x)J'_l(y)$.

Multiplying left and right parts of the equation (27) by the functions $\cos[l_1(p)(\phi-\gamma/2)]$, $p = 0,1,2,...$ and integrating the result at the interval $[\gamma/2;\ (\pi-\gamma)/2]$, at which the system of these functions is orthogonal, we obtain:

$$\sum_{m=0}^{\infty} B_m I_1(p,m) J'Y'[l_2(m), k_c b, k_c d] =$$
$$= A_p(\pi - 2\gamma)/4(1+\delta_{p0}) J'Y'[l_1(p), k_c a, k_c d], \quad (30)$$

whence the amplitude of the p-th partial mode in the region I (Fig. 2) is defined as follows

$$A_p = \frac{4\sum_{m=0}^{\infty} B_m I_1(p,m) J'Y'[l_2(m), k_c b, k_c d]}{(\pi - 2\gamma)(1+\delta_{p0}) J'Y'[l_1(p), k_c a, k_c d]}. \quad (31)$$

In the formulas (30), (31), the following designations are used:

$$I_1(p,m) = \int_{\gamma/2}^{(\pi-\gamma)/2} \sin[l_2(m)\phi]\cos[l_1(p)(\phi - \gamma/2)]\mathrm{d}\phi;$$

δ_{p0} is the Kronecker delta.

In the same way, the amplitude of the p-th partial mode in the region I (Fig. 2) can be derived from the expression (28)

$$A_p = \frac{4\sum_{m=0}^{\infty} B_m I_1(p,m) J'Y[l_2(m), k_c b, k_c d]}{(\pi - 2\gamma)(1+\delta_{p0}) J'Y[l_1(p), k_c a, k_c d]}. \quad (32)$$

Having equated (31) and (32), one can obtain

$$\sum_{m=0}^{\infty} B_m I_1(p,m)\{\frac{J'Y'[l_2(m), k_c b, k_c d]}{J'Y'[l_1(p), k_c a, k_c d]} -$$
$$-\frac{J'Y[l_2(m), k_c b, k_c d]}{J'Y[l_1(p), k_c a, k_c d]}\} = 0. \quad (33)$$

By simplifying the expression (33), we obtain

$$\sum_{m=0}^{\infty} B_m F_1(p,m,k_c a, k_c b, k_c d) = 0, \ p = 0,1,2,\ldots, \quad (34)$$

where $F_1(p,m,x,y,z) = I_1(p,m) \times$
$$\times\left[\frac{J'Y'(l_2(m),y,z)}{J'Y'(l_1(p),x,z)} - \frac{J'Y(l_2(m),y,z)}{J'Y(l_1(p),x,z)}\right].$$

Multiplying left and right parts of the equation (29) by the system of functions $\sin[l_2(q)\phi]$, $q = 0,1,2,\ldots$ and integrating the resulting relation at the disjunction of intervals $[0;\ \gamma/2] \cup [(\pi-\gamma)/2;\ \pi/2]$, we get

$$\sum_{m=0}^{\infty} B_m I_2(q,m) J'Y'[l_2(m), k_c b, k_c d] = 0, \quad (35)$$

where $I_2(q,m) = \int_0^{\gamma/2} \sin[l_2(m)\phi]\sin[l_2(q)\phi]\mathrm{d}\phi +$
$$\int_{(\pi-\gamma)/2}^{\pi/2} \sin[l_2(m)\phi]\sin[l_2(q)\phi]\mathrm{d}\phi.$$

Simplifying the expression (35) yields the following result:

$$\sum_{m=0}^{\infty} B_m F_2(q,m,k_c b, k_c d) = 0, \ q = 0,1,2,\ldots, \quad (36)$$

where $F_2(q,m,y,z) = I_2(q,m) J'Y'[l_2(m), y, z]$.

Having united the systems of equations (34), (36) and limiting the number of partial modes in the region II, we obtain the following homogeneous SLAE with unknown partial mode amplitudes B_m:

$$\begin{cases} \sum_{m=0}^{M-1} B_m F_1(p,m,k_c a, k_c b, k_c d) = 0, p = 0,1,\ldots,(P-1) \\ \sum_{m=0}^{M-1} B_m F_2(q,m,k_c b, k_c d) = 0, q = 0,1,\ldots,(M-P-1) \end{cases} \quad (37)$$

At fixed number of partial modes M, the number of equations of the first type is defined by the angular widths ratio of the regions I and II (Fig. 2) as $P = \mathrm{int}[\pi - 2\gamma)/\pi M]$, where integer part is rounded up or down [27].

The SLAE (37) can be rewritten in the matrix form by the formula (19), but the matrix $[F]$ elements are different:

$$F(i,j) = \begin{cases} F_1(i,j,k_c a, k_c b, k_c d), & i = 0,1,\ldots,(P-1) \\ F_2((i-P), j, k_c b, k_c d), & i = P,(P+1),\ldots,(M-1) \end{cases}.$$

The condition of nontrivial solution of the homogeneous SLAE (37) is the equality to zero of the matrix $[F]$ determinant. This condition defines the cutoff mode numbers of TE modes. The cutoff wave numbers calculated are to be substituted in homogeneous SLAE (37). The further solution of the TE modes problem is the same as the one described hereinbefore for the TEM mode except for the calculation of electric and magnetic fields components distributions. The distributions of longitudinal component of magnetic field H_z in the regions I and II (Fig. 2) can be defined by the formulas (20), (21). The magnetic field solution for the entire cross section of CQRW is found by using the symmetry or the antisymmetry properties of the TE modes. Transversal components of magnetic and electric fields are defined by using the formulas (38)–(41) connecting longitudinal and transversal field components (in which for the TE modes $E_z \equiv 0$):

$$E_r(r,\phi) = -\frac{i\beta}{k_c^2}\frac{\partial E_z(r,\phi)}{\partial r} - \frac{Z(f,k_c)}{k_c r}\frac{\partial H_z(r,\phi)}{\partial \phi}; \quad (38)$$

$$E_\phi(r,\phi) = -\frac{i\beta}{k_c^2 r}\frac{\partial E_z(r,\phi)}{\partial \phi} + \frac{Z(f,k_c)}{k_c}\frac{\partial H_z(r,\phi)}{\partial r}; \quad (39)$$

$$H_r(r,\phi) = -\frac{i\beta}{k_c^2}\frac{\partial H_z(r,\phi)}{\partial r} + \frac{Y(f,k_c)}{k_c r}\frac{\partial E_z(r,\phi)}{\partial \phi}; \quad (40)$$

$$H_\phi(r,\phi) = -\frac{i\beta}{k_c^2 r}\frac{\partial H_z(r,\phi)}{\partial \phi} - \frac{Y(f,k_c)}{k_c}\frac{\partial E_z(r,\phi)}{\partial r}, \quad (41)$$

where $Y(f,k_c) = 2\pi i f\varepsilon_a / k_c$; β denotes the longitudinal mode number of CQRW; i designates an imaginary unit; f is the operating frequency; ε_a defines the absolute permittivity of CQRW inner medium.

TE modes symmetric relative to the plane $\varphi = \pi/2$

In the regions I and II (Fig. 3), we represent the fields H_z and E_ϕ in the form of infinite sums (20)–(23) of the partial modes with unknown amplitudes and cutoff wave numbers. Each partial mode satisfies the Maxwell equations in the cylindrical coordinate system and boundary conditions at the two magnetic walls or at the magnetic and electric walls as well as at the perfectly conducting surfaces of CQRW, where $l_1(n) = 4\pi n/(\pi - 2\gamma)$, $l_2(m) = 4m + 2$ for the TE modes with antisymmetric EFD relative to the plane $\phi = \pi/4$ (for which this plane is the electric wall) or $l_1(n) = 2\pi(2n+1)/(\pi - 2\gamma)$, $l_2(m) = 4m + 4$ for the TE modes with symmetric EFD relative to the plane $\phi = \pi/4$ (for which this plane is the magnetic wall).

The boundary conditions at the interface between the regions I and II (Fig. 3) are as follows:

$$E_\phi^{II}(r = d,\ \phi \in [\gamma/2; \pi/4]) = E_\phi^{I}(r = d,\ \phi \in [\gamma/2; \pi/4]); \quad (42)$$

$$H_z^{II}(r = d,\ \phi \in [\gamma/2; \pi/4]) = H_z^{I}(r = d,\ \phi \in [\gamma/2; \pi/4]). \quad (43)$$

Besides, there is the following relation at the perfectly conducting surface of the ridge at $r = d$ and $\varphi \in [0; \gamma/2]$:

$$E_\phi^{II}(r = d,\ \phi \in [0;\ \gamma/2]) = 0. \quad (44)$$

Substituting (20)–(23) in (42)–(44) yields the results:

$$\sum_{m=0}^{\infty} B_m \sin[l_2(m)\phi] J'Y'[l_2(m), k_c b, k_c d] = \sum_{n=0}^{\infty} A_n \cos[l_1(n)(\phi - \gamma/2)] J'Y'[l_1(n), k_c a, k_c d],$$
$$\varphi \in [\gamma/2; \pi/4]; \quad (45)$$

$$\sum_{m=0}^{\infty} B_m \sin[l_2(m)\phi] J'Y[l_2(m), k_c b, k_c d] = \sum_{n=0}^{\infty} A_n \cos[l_1(n)(\phi - \gamma/2)] J'Y[l_1(n), k_c a, k_c d],$$
$$\varphi \in [\gamma/2; \pi/4]; \quad (46)$$

$$\sum_{m=0}^{\infty} B_m \sin[l_2(m)\phi] J'Y'[l_2(m), k_c b, k_c d] = 0,$$
$$\varphi \in [0; \gamma/2]. \quad (47)$$

Multiplying left and right parts of the equation (45) by the system of functions $\cos[l_1(p)(\phi - \gamma/2)]$, $p = 0,1,2,...$ and integrating the resulting relation at the interval $[\gamma/2; \pi/4]$, at which the system of these functions is orthogonal, we obtain:

$$\sum_{m=0}^{\infty} B_m I_1(p,m) J'Y'[l_2(m), k_c b, k_c d] = A_p \frac{\pi - 2\gamma}{8}(1 + \delta_{p0}) J'Y'[l_1(p), k_c a, k_c d] \quad (48)$$

for the TE modes with antisymmetric EFD relative to the plane $\phi = \pi/4$;

$$\sum_{m=0}^{\infty} B_m I_1(p,m) J'Y'[l_2(m), k_c b, k_c d] = A_p \frac{\pi - 2\gamma}{8} J'Y'[l_1(p), k_c a, k_c d] \quad (49)$$

for the TE modes with symmetric EFD relative to the plane $\phi = \pi/4$.

By using relations (48), (49), the amplitude of the p-th partial mode in the region I (Fig. 3) can be obtained:

$$A_p = \frac{8\sum_{m=0}^{\infty} B_m I_1(p,m) J'Y'[l_2(m), k_c b, k_c d]}{(\pi - 2\gamma)(1 + \delta_{p0}) J'Y'[l_1(p), k_c a, k_c d]}, \quad (50)$$

for the TE modes with antisymmetric EFD relative to the plane $\phi = \pi/4$;

$$A_p = \frac{8\sum_{m=0}^{\infty} B_m I_1(p,m) J'Y'[l_2(m), k_c b, k_c d]}{(\pi - 2\gamma) J'Y'[l_1(p), k_c a, k_c d]}. \quad (51)$$

for the TE modes with symmetric EFD relative to the plane $\phi = \pi/4$.

In the formulas (48)–(51), we have believed that

$$I_1(p,m) = \int_{\gamma/2}^{\pi/4} \sin[l_2(m)\phi]\cos[l_1(p)(\phi - \gamma/2)]\mathrm{d}\phi.$$

In the same way, the amplitude of the p-th partial mode in the region I (Fig. 3) can be derived from (46):

$$A_p = \frac{8\sum_{m=0}^{\infty} B_m I_1(p,m) J'Y[l_2(m), k_c b, k_c d]}{(\pi - 2\gamma)(1+\delta_{p0}) J'Y[l_1(p), k_c a, k_c d]} \quad (52)$$

for the TE modes with antisymmetric EFD relative to the plane $\phi = \pi/4$;

$$A_p = \frac{8\sum_{m=0}^{\infty} B_m I_1(p,m) J'Y[l_2(m), k_c b, k_c d]}{(\pi - 2\gamma) J'Y[l_1(p), k_c a, k_c d]} \quad (53)$$

for the TE modes with symmetric EFD relative to the plane $\phi = \pi/4$.

Having equated (50) to (52) or (51) to (53) one can obtain (33) and (34) received in the previous section.

Next we multiply left and right parts of the equation (47) by the system of functions $\sin[l_2(q)\phi]$, $q = 0,1,2...$, and integrate the resulting relation at the interval $[0;\ \gamma/2]$. As a result, we obtain (35), where

$$I_2(q,m) = \int_0^{\gamma/2} \sin[l_2(m)\phi]\sin[l_2(q)\phi]\mathrm{d}\phi.$$

The further course of solving the problem is the same as that described in the previous section.

TM modes antisymmetric relative to the plane $\varphi = \pi/2$

The TM eigenmodes designations introduced in this section coincide with the ones given above for the TEM mode and the TE modes. In the regions I and II (Fig. 2), we represent the fields E_z and H_ϕ in the form of infinite sums of the partial modes with unknown amplitudes and cutoff wave numbers, each of which satisfies the Maxwell equations in the cylindrical coordinate system and boundary conditions at the magnetic, electric walls as well as at the perfectly conducting surfaces of CQRW (see Fig. 2):

$$E_z^{\mathrm{I}}(r,\phi) = \sum_{n=0}^{\infty} A_n \sin[l_1(n)(\phi - \gamma/2)] \times$$
$$\times [J_{l_1(n)}(k_c a) Y_{l_1(n)}(k_c r) - Y_{l_1(n)}(k_c a) J_{l_1(n)}(k_c r)]; \quad (54)$$

$$E_z^{\mathrm{II}}(r,\phi) = \sum_{m=0}^{\infty} B_m \cos[l_2(m)\phi] \times$$
$$\times [J_{l_2(m)}(k_c b) Y_{l_2(m)}(k_c r) - Y_{l_2(m)}(k_c b) J_{l_2(m)}(k_c r)]; \quad (55)$$

$$H_\phi^{\mathrm{I}}(r,\phi) = Y(f,k_c) \sum_{n=0}^{\infty} A_n \sin[l_1(n)(\phi - \gamma/2)] \times$$
$$\times [J_{l_1(n)}(k_c a) Y'_{l_1(n)}(k_c r) - Y_{l_1(n)}(k_c a) J'_{l_1(n)}(k_c r)]; \quad (56)$$

$$H_\phi^{\mathrm{II}}(r,\phi) = Y(f,k_c) \sum_{m=0}^{\infty} B_m \cos[l_2(m)\phi] \times$$
$$\times [J_{l_2(m)}(k_c b) Y'_{l_2(m)}(k_c r) - Y_{l_2(m)}(k_c b) J'_{l_2(m)}(k_c r)], \quad (57)$$

where $l_1(n) = 2\pi(n+1)/(\pi - 2\gamma)$; $l_2(m) = 2m+1$; A_n and B_m are unknown amplitude coefficients, $J_l(x)$, $Y_l(x)$, $J'_l(x)$, $Y'_l(x)$ are Bessel functions of the first and the second kind and their derivatives, k_c is a cutoff wave number.

The boundary conditions at the interface between the regions I and II (Fig. 2) are as follows:

$$E_z^{\mathrm{II}}(r = d,\ \phi \in [\gamma/2;\ (\pi - \gamma)/2]) =$$
$$= E_z^{\mathrm{I}}(r = d,\ \phi \in [\gamma/2;\ (\pi - \gamma)/2]); \quad (58)$$

$$H_\phi^{\mathrm{II}}(r = d,\ \phi \in [\gamma/2;\ (\pi - \gamma)/2]) =$$
$$= H_\phi^{\mathrm{I}}(r = d,\ \phi \in [\gamma/2;\ (\pi - \gamma)/2]). \quad (59)$$

Besides, at the perfectly conducting surfaces of ridges at $r = d$ and $\phi \in [0;\ \gamma/2] \cup [(\pi - \gamma)/2;\ \pi/2]$:

$$E_z^{\mathrm{II}}(r = d,\ \phi \in [0;\ \gamma/2] \cup [(\pi - \gamma)/2;\ \pi/2]) = 0. \quad (60)$$

Substituting (54)–(57) in (58)–(60), we obtain

$$\sum_{m=0}^{\infty} B_m \cos[l_2(m)\phi] JY[l_2(m), k_c b, k_c d] =$$
$$= \sum_{n=0}^{\infty} A_n \sin[l_1(n)(\phi - \gamma/2)] JY[l_1(n), k_c a, k_c d],$$
$$\phi \in [\gamma/2;\ (\pi - \gamma)/2]; \quad (61)$$

$$\sum_{m=0}^{\infty} B_m \cos[l_2(m)\phi] JY'[l_2(m), k_c b, k_c d] =$$
$$= \sum_{n=0}^{\infty} A_n \sin[l_1(n)(\phi - \gamma/2)] JY'[l_1(n), k_c a, k_c d],$$
$$\phi \in [\gamma/2;\ (\pi - \gamma)/2]; \quad (62)$$

$$\sum_{m=0}^{\infty} B_m \cos[l_2(m)\phi] JY[l_2(m), k_c b, k_c d] = 0,$$
$$\phi \in [0;\ \gamma/2] \cup [(\pi-\gamma)/2;\ \pi/2], \quad (63)$$

where $JY(l,x,y) = J_l(x)Y_l(y) - Y_l(x)J_l(y)$, $JY'(l,x,y) = J_l(x)Y_l'(y) - Y_l(x)J_l'(y)$.

Multiplying left and right parts of the equation (61) by the system of functions $\sin[l_1(p)(\phi-\gamma/2)]$, $p = 0,1,2,...$ and integrating the result at the interval $[\gamma/2;\ (\pi-\gamma)/2]$, at which the system of these functions is orthogonal, we obtain

$$\sum_{m=0}^{\infty} B_m I_1(p,m) JY[l_2(m), k_c b, k_c d] =$$
$$= A_p \frac{\pi-2\gamma}{4} JY(l_1(p), k_c a, k_c d), \quad (64)$$

whence it follows, that the amplitude of the p-th partial mode in the region I (Fig. 2) is expressed as

$$A_p = \frac{4\sum_{m=0}^{\infty} B_m I_1(p,m) JY[l_2(m), k_c b, k_c d]}{(\pi-2\gamma) JY[l_1(p), k_c a, k_c d]}. \quad (65)$$

In the formulas (64), (65), the following designation is assumed

$$I_1(p,m) = \int_{\gamma/2}^{(\pi-\gamma)/2} \cos[l_2(m)\phi] \sin[l_1(p)(\phi-\gamma/2)] d\phi.$$

In the same way, the amplitude of the p-th partial mode in the region I (Fig. 2) can be obtained from (62). As a result, we get

$$A_p = \frac{4\sum_{m=0}^{\infty} B_m I_1(p,m) JY'[l_2(m), k_c b, k_c d]}{(\pi-2\gamma) JY'[l_1(p), k_c a, k_c d]}. \quad (66)$$

Having equated (65) to (66), one can easily obtain

$$\sum_{m=0}^{\infty} B_m I_1(p,m) \{\frac{JY[l_2(m), k_c b, k_c d]}{JY[l_1(p), k_c a, k_c d]} -$$
$$- \frac{JY'[l_2(m), k_c b, k_c d]}{JY'[l_1(p), k_c a, k_c d]}\} = 0. \quad (67)$$

Let us introduce the following designation:

$$F_1(p,m,x,y,z) = I_1(p,m)\{\frac{JY[l_2(m), y, z]}{JY[l_1(p), x, z]} -$$
$$- \frac{JY'[l_2(m), y, z]}{JY'[l_1(p), x, z]}\}.$$

Using this designation, the relation (67) can be rewritten by the formula (34).

Next, we multiply left and right parts of the equation (63) by the system of functions $\cos[l_2(q)\phi]$, $q = 0,1,2,...$ and integrate the result at the disjunction of intervals $[0;\ \gamma/2] \cup [(\pi-\gamma)/2;\ \pi/2]$. In the issue, we obtain

$$\sum_{m=0}^{\infty} B_m I_2(q,m) JY[l_2(m), k_c b, k_c d] = 0, \quad (68)$$

where $I_2(q,m) = \int_0^{\gamma/2} \cos[l_2(m)\phi]\cos[l_2(q)\phi] d\phi +$
$\int_{(\pi-\gamma)/2}^{\pi/2} \cos[l_2(m)\phi]\cos[l_2(q)\phi] d\phi$.

Introducing the designation $F_2(q,m,y,z) = I_2(q,m) JY[l_2(m), y, z]$, we can rewrite (68) by the formula (36). The further way of solving the problem is the same as that described hereinbefore for the TE eigenmodes.

TM modes symmetric relative to the plane $\varphi = \pi/2$

In the regions I and II (Fig. 3), we represent the fields E_z and H_ϕ in the form of infinite sums (54)–(57) of the partial modes with unknown amplitudes and cutoff wave numbers, each of which satisfies the Maxwell equations in the cylindrical coordinate system as well as boundary conditions at the two magnetic walls or at the magnetic and electric walls and at the perfectly conducting surfaces of CQRW, where $l_1(n) = 4\pi(n+1)/(\pi-2\gamma)$, $l_2(m) = 4m+2$ for the TM modes with antisymmetric EFD relative to the plane $\phi = \pi/4$ (for them this plane is the electric wall) or $l_1(n) = 2\pi(2n+1)/(\pi-2\gamma)$, $l_2(m) = 4m$ for the TM modes with symmetric EFD relative to the plane $\phi = \pi/4$ (for them this plane is the magnetic wall).

The boundary conditions at the interface between the regions I and II (Fig. 3) are as follows:

$$E_z^{II}(r=d,\ \phi \in [\gamma/2;\ \pi/4]) =$$
$$= E_z^{I}(r=d,\ \phi \in [\gamma/2;\ \pi/4]); \quad (69)$$
$$H_\phi^{II}(r=d,\ \phi \in [\gamma/2;\ \pi/4]) =$$
$$= H_\phi^{I}(r=d,\ \phi \in [\gamma/2;\ \pi/4]). \quad (70)$$

Besides, at the perfectly conducting surface of the ridge at $r = d$ and $\phi \in [0;\ \gamma/2]$ we have:

$$E_z^{II}(r=d,\ \phi \in [0;\ \gamma/2]) = 0. \quad (71)$$

Having substituted (54)–(57) in (69)–(71), we obtain:

$$\sum_{m=0}^{\infty} B_m \cos[l_2(m)\phi] JY[l_2(m), k_c b, k_c d] = \\ = \sum_{n=0}^{\infty} A_n \sin[l_1(n)(\phi - \gamma/2)] JY[l_1(n), k_c a, k_c d], \\ \phi \in [\gamma/2;\ \pi/4]; \quad (72)$$

$$\sum_{m=0}^{\infty} B_m \cos[l_2(m)\phi] JY'[l_2(m), k_c b, k_c d] = \\ = \sum_{n=0}^{\infty} A_n \sin[l_1(n)(\phi - \gamma/2)] JY'[l_1(n), k_c a, k_c d], \\ \phi \in [\gamma/2;\ \pi/4]; \quad (73)$$

$$\sum_{m=0}^{\infty} B_m \cos[l_2(m)\phi] JY[l_2(m), k_c b, k_c d] = 0, \\ \phi \in [0;\ \gamma/2]. \quad (74)$$

Multiplying left and right parts of the equation (72) by the system of functions $\sin[l_1(p)(\phi - \gamma/2)]$, $p = 0,1,2,...$ and integrating the result at the interval $[\gamma/2;\ \pi/4]$, at which the system of these functions is orthogonal, we obtain

$$\sum_{m=0}^{\infty} B_m I_1(p,m) JY[l_2(m), k_c b, k_c d] = \\ = A_p \frac{\pi - 2\gamma}{4} JY[l_1(p), k_c a, k_c d], \quad (75)$$

whence it follows that the amplitude of the p-th partial mode in the region I (Fig. 3) can be found as

$$A_p = \frac{4\sum_{m=0}^{\infty} B_m I_1(p,m) JY[l_2(m), k_c b, k_c d]}{(\pi - 2\gamma) JY[l_1(p), k_c a, k_c d]}. \quad (76)$$

It is assumed that in the formulas (75), (76)

$$I_1(p,m) = \int_{\gamma/2}^{\pi/4} \cos[l_2(m)\phi] \sin[l_1(p)(\phi - \gamma/2)] d\phi.$$

In the same way, the amplitude of the p-th partial mode in the region I (Fig. 3) can be obtained from the expression (73)

$$A_p = \frac{4\sum_{m=0}^{\infty} B_m I_1(p,m) JY'[l_2(m), k_c b, k_c d]}{(\pi - 2\gamma) JY'[l_1(p), k_c a, k_c d]}. \quad (77)$$

Having equated (76) to (77), one can easily obtain (67) and (34).

Next, multiplying left and right parts of the equation (74) by the system of functions $\cos[l_2(q)\phi]$, $q = 0,1,2,...$ and integrating the result at the interval $[0;\ \gamma/2]$, we obtain (68), where

$$I_2(q,m) = \int_0^{\gamma/2} \cos[l_2(m)\phi] \cos[l_2(q)\phi] d\phi.$$

The further way of solving the problem is the same as that described in the previous section.

Convergence of cutoff wave number solutions

In this section we carry out the convergence analysis of cutoff wave number solutions depending on the number of partial modes M limiting the sums in (18), (37). The calculations have been performed for the both CQRW configurations depicted in Fig. 1. As can be seen in this Figure, for both configurations of CQRW the regions I and III are bounded by the three perfectly conducting surfaces of CQRW and by the interface of regions. The region II is bounded by two magnetic walls, by four perfectly conducting surfaces of CQRW and by two interfaces between the regions. Therefore, all formulas remain the same for both configurations.

For the CQRW with ridges on inner cylinder we set the ridges angle and dimensions ratios as follows: γ = 10°, 30°, 50°, a/b = 0.5, $(b-d)/b$ = 0.1, and for the CQRW with ridges on outer cylinder: γ = 10°, 30°, 50°, b/a = 0.5, $(d-b)/a$ = 0.1. Residual errors δ ($\delta = [k_c(M) - k_c(30)]/k_c(30) \times 100\%$) plots for cutoff wave numbers of the first three TE modes and the first TM mode of CQRW versus the number of partial modes M are shown in Fig. 4–6. Herewith residual errors for the first, the second, the third TE modes and for the first TM mode are shown by solid, dashed, dash-dotted and dotted lines respectively. The results for the CQRW with ridges on inner cylinder are shown in Fig. 4*a*–6*a*, and the ones for the CQRW with ridges on outer cylinder are depicted in Fig. 4*b*–6*b*. The residual errors are calculated relative to the cutoff wave numbers obtained at M = 30.

As can be seen in Figures 4–6, the residual errors for cutoff wave numbers decrease as the ridges angle γ increases. Having compared Fig. 4*a*–6*a* with Fig. 4*b*–6*b*, one can see that the residual errors of cutoff wave numbers of the first three TE modes for the CQRW with ridges on outer cylinder are less than the ones for the CQRW with ridges on inner cylinder for the same relative value of the gaps between ridges and perfectly conducting circular cylinder. For the first TM mode these residual errors are almost the same for both CQRW configurations.

As one can see in Fig. 4–6, taking into account 27 partial modes provides the residual errors of cutoff wave numbers of the first three TE modes and the first TM mode less than 0.1 % comparatively with the values of cutoff wave numbers obtained in the case of 30 partial modes. Consequently, it is enough to use 27 partial modes for the calculation of the CQRW cutoff wave numbers for both configurations by the transverse field-matching technique with the residual error less than 0.1%.

Convergence of electric field solutions

Now we analyze solutions convergence of EFD for the TEM mode and the first TE mode depending on the number of partial modes M limiting the sums in (18), (37). The calculations have been performed for both CQRW configurations depicted in Fig. 1 with the same dimensions ratios as the ones that were set during the solutions convergence analysis for cutoff wave numbers and the angle γ = 30°. The TEM mode's EFD are shown in Fig. 7, 8, and EFD of the first TE mode are depicted in Fig. 9, 10. The electric field radial component's distributions $E_r(r = d, \varphi \in [0; \pi])$ computed at the interface between the regions I, II and III (see Fig. 1) are presented in Fig. 7, 9, and the distributions for the azimuthal one $E_\varphi(r = d, \varphi \in [0; \pi])$ are shown in Fig. 8, 10. In Fig. 7–10 the results obtained utilizing 10, 20, 30 partial modes are shown by dotted, dashed and solid lines respectively.

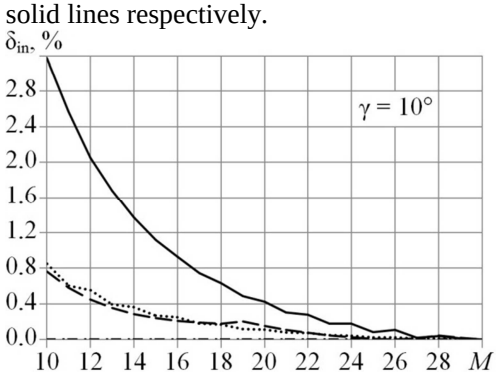

(*a*)

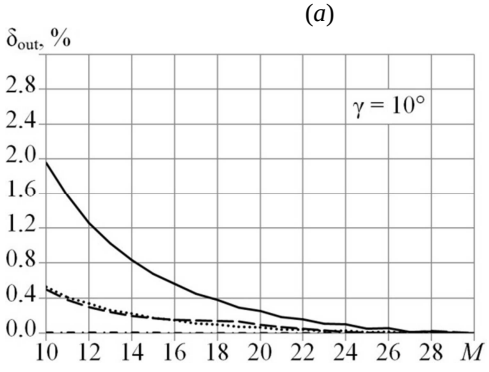

(*b*)

Fig. 4. Cutoff wave numbers residual errors versus the number of partial modes for coaxial quad-ridged waveguides with ridges: (*a*) on inner conducting circular cylinder; (*b*) on outer conducting circular cylinder.

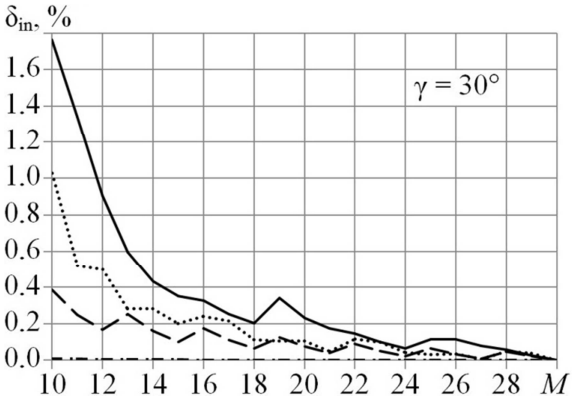

(*a*)

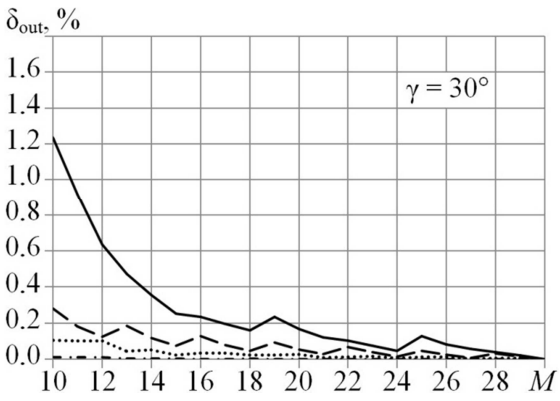

(*b*)

Fig. 5. Cutoff wave numbers residual errors versus the number of partial modes for coaxial quad-ridged waveguides with ridges: (*a*) on inner conducting circular cylinder; (*b*) on outer conducting circular cylinder.

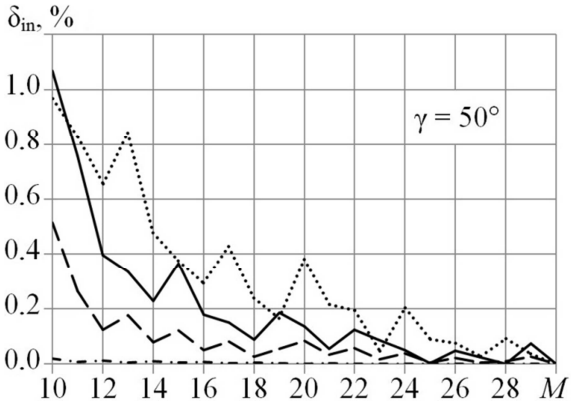

(*a*)

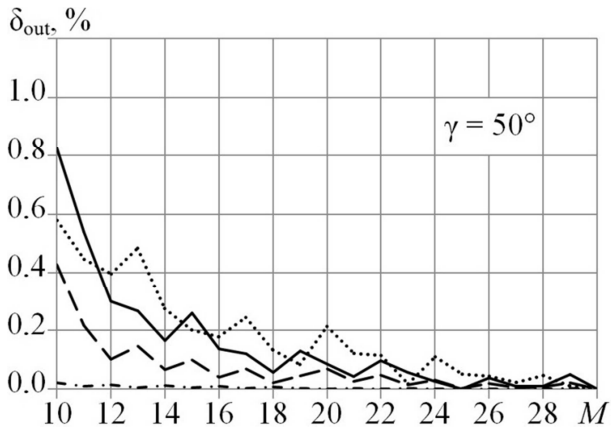

(*b*)

Fig. 6. Cutoff wave numbers residual errors versus the number of partial modes for coaxial quad-ridged waveguides with ridges: (*a*) on inner conducting circular cylinder; (*b*) on outer conducting circular cylinder.

As one can see in Fig. 7–10, the EFD becomes more narrow and sharp in the vicinity of the peak values as the number of partial modes M increases. These sharp rises of electric field are caused by the singularity of the field's behavior at the ridge. The more partial modes are used in the EFD computing, the more accurate their sum approximates this singularity. The field behavior in the vicinity of the ridges' edges and in the gaps between the ridges and circular cylinders of CQRW for both configurations is in good agreement with the behavior of electric field of the fundamental TE mode of sectoral coaxial ridged waveguides [26].

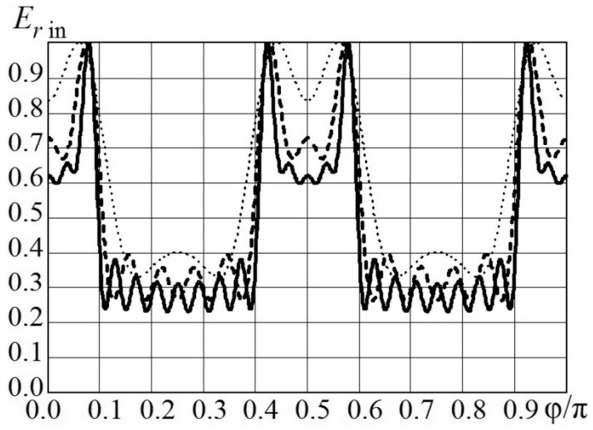

(*a*)

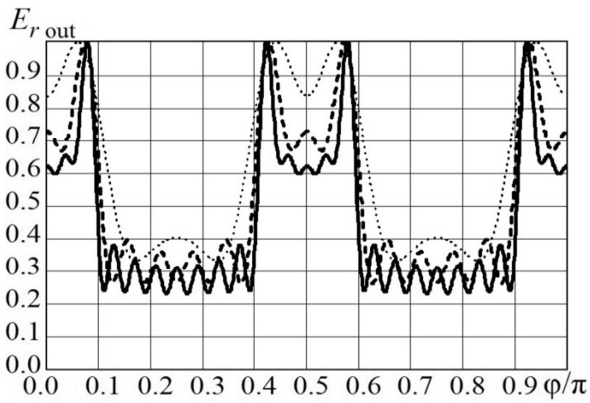

(*b*)

Fig. 7. TEM mode electric field radial component distribution for coaxial quad-ridged waveguides with ridges: (*a*) on inner conducting circular cylinder; (*b*) on outer conducting circular cylinder (parameter is a number of partial modes *M*).

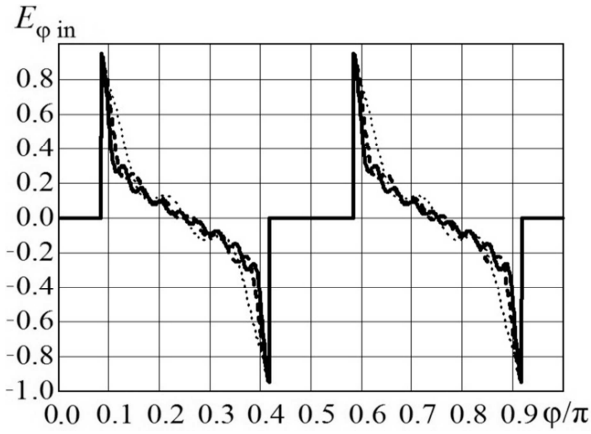

(*a*)

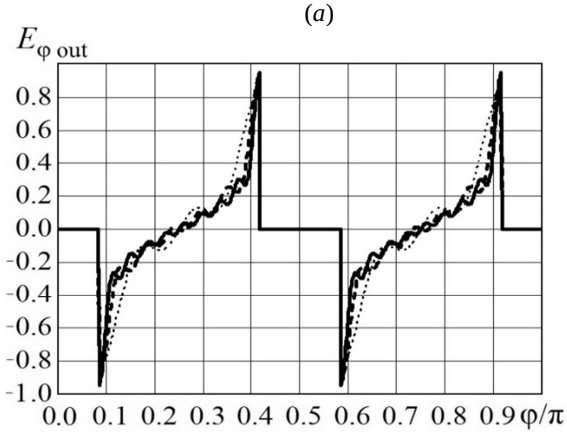

(*b*)

Fig. 8. TEM mode electric field azimuthal component distribution for coaxial quad-ridged waveguides with ridges: (*a*) on inner conducting circular cylinder; (*b*) on outer conducting circular cylinder (parameter is a number of partial modes *M*).

As one can see in Fig. 9, 10, for the first TE mode in CQRW the electric field components distributions converge sufficiently fast and depend on the number of used partial modes weakly. The different situation is observed for the EFD of the TEM mode (see Fig. 7, 8). In the case of using of 10 or 20 partial modes the distribution of the radial electric field component E_r of the TEM mode in the vicinity of the gap between the ridge and the circular cylinder of CQRW is not as uniform as in the case of utilizing of 30 partial modes. This distribution should be close to the uniform one, because the behavior of the radial electric field component in the gap between the ridge and the cylindrical surface is the same as for the fundamental TE mode of sectoral coaxial ridged waveguides [26]. Consequently, for the correct calculation of CQRW modes' field distributions by transverse field-matching technique one should utilize more than 30 partial modes.

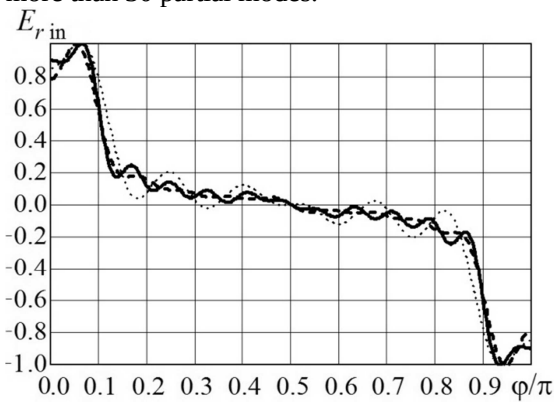

(*a*)

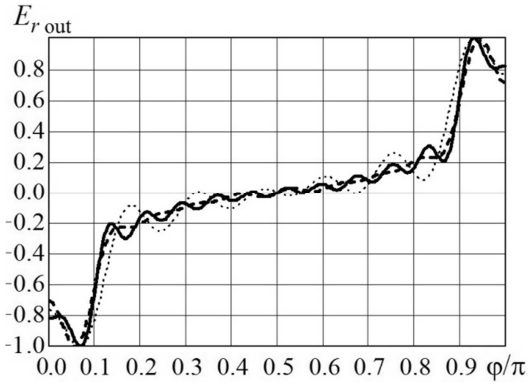

(*b*)

Fig. 9. The first TE mode electric field radial component distribution for coaxial quad-ridged waveguides with ridges: (*a*) on inner conducting circular cylinder; (*b*) on outer conducting circular cylinder (parameter is a number of partial modes *M*).

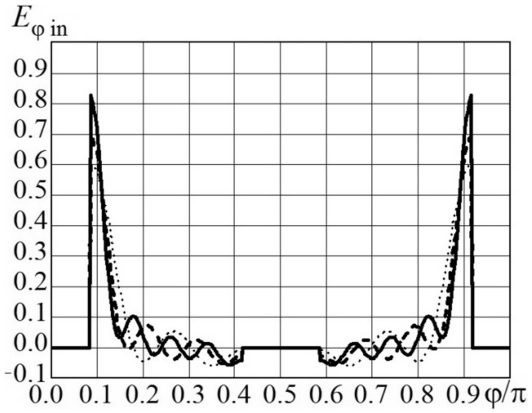

(*a*)

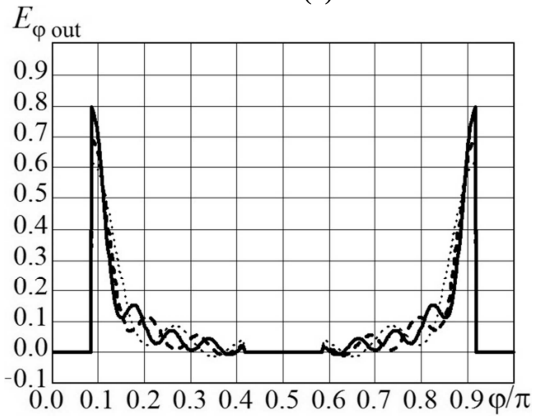

(*b*)

Fig. 10. The first TE mode electric field azimuthal component distribution for coaxial quad-ridged waveguides with ridges: (*a*) on inner conducting circular cylinder; (*b*) on outer conducting circular cylinder (parameter is a number of partial modes *M*).

Conclusion

The boundary problem for eigenmodes in coaxial quad-ridged waveguides has been solved by transverse field-matching technique. The formulas obtained provide possibilities to compute cutoff wave numbers and electric and magnetic fields distributions for the TEM, the TE and the TM modes in the presence of the ridges either on the inner or on the outer perfectly conducting cylinder. It has been shown that for the calculation of cutoff wave numbers by transverse field-matching technique with residual error less than 0.1 % it is enough to utilize 27 partial modes, and for the correct calculation of the field distributions one should utilize more than 30 partial modes.

References

1. Suntheralingam N., Mohottige N., Budimir D. Electromagnetic modelling of ridged waveguide resonator loaded bandpass filters // 2010 IEEE Antennas and Propagation Society International Symposium (APSURSI 2010), Toronto, Canada, 2010, pp. 1–4.
2. Li S., Fu J., Wu X. Double ridged waveguide low pass filters for satellite application // 2007 International Symposium on Microwave, Antenna, Propagation and EMC Technologies for Wireless Communications, Hangzhou, China, 2007, pp. 408–410.
3. Manuilov M. B., Kobrin K. V., Obrezanova L. A. Ridged waveguide filters with improved performance // 16th International Crimean Conference on Microwave and Telecommunication Technology (CriMiCo 2006), Sevastopol, Ukraine, 2006, pp. 507–508.
4. Dai D., Wang Z., Julian N., Bowers J. E. Compact broadband polarizer based on shallowly-etched silicon-on-insulator ridge optical waveguides // 2011 Optical Fiber Communication and National Fiber Optic Engineers Conference (OFC/NFOEC), Los Angeles, USA, 2011, pp. 1–3.
5. Tribak A., Mediavilla A., Cano J. L., Boussouis M., Cepero K. Ultra-broadband low axial ratio corrugated quad-ridge polarizer // European Microwave Conference (EuMC 2009), Rome, Italy, 2009, pp. 73–76.
6. Bull J. D., Kato H., Jaeger N. Asymmetrically strained ridge waveguide for passive polarization conversion // IEEE Photonics Technology Letters. – Dec. 2008. – vol. 20, № 24. – pp. 2186–2188.
7. Polemi A., Maci S., Kildal P.-S. Dispersion characteristics of a metamaterial-based parallel-plate ridge gap waveguide realized by bed of nails // IEEE Trans. Antennas Propagat. – March 2011. – vol. 59, № 3 – pp. 904–913.
8. Ruiz-Bernal M. A., Valverde-Navarro M., Goussetis G., Gomez-Tornero J.-L., Feresidis A. P. Higher order modes of the ridged coaxial waveguide // 36th European Microwave Conference, Manchester, UK, 2006, pp. 1221–1224.
9. Tang Y., Zhao J., Wu W. Analysis of quadruple-ridged square waveguide by multilayer perceptron neural network model // Asia-Pacific Microwave Conference (APMC 2006), Yokohama, Japan, 2006, pp. 1912–1918.
10. Xu J., Wang W., Gong Y., Wei Y. Analysis of elliptical ridged waveguide // Joint 31st International Conference on Infrared Millimeter Waves and 14th International Conference on Teraherz Electronics (IRMMW-THz 2006), Shanghai, China, 2006, p. 265.
11. Jacobs O. B., Odendaal J. W., Joubert J. Elliptically shaped quad-ridge horn antennas as feed for a reflector // IEEE Antennas Wireless Propagat. Lett. – 2011. – vol. 10. – pp. 756–759.
12. Akgiray A., Weinreb S., Imbriale W. Design and measurements of dual-polarized wideband constant-beamwidth quadruple-ridged flared horn // 2011 IEEE International Symposium on Antennas and Propagation (APSURSI 2011), Spokane, USA, 2011, pp. 1135–1138.
13. Jacobs O. B., Odendaal J. W., Joubert J. Quad ridge horn antenna with elliptically shaped sidewalls // 2011 International Conference on Electromagnetics in Advanced Applications (ICEAA 2011), Torino, Italy, 2011, pp. 259–262.
14. Coutts G. M. Wideband diagonal quadruple-ridge orthomode transducer for circular polarization detection // IEEE Trans. Antennas Propagat.– June 2011.– vol. 59, № 6 – pp. 1902–1909.
15. Hwang J.-H., Oh Y. Compact orthomode transducer using single-ridged triangular waveguides // IEEE Microwave Wireless Comp. Lett. – 2011. – vol. 21, № 8 – pp. 412–414.
16. Zhang H. Z. A wideband orthogonal-mode junction using ridged sectoral waveguides // 2002 IEEE Int. Antennas Propagat. Symp. Dig. – June 2002. – vol. 40. – pp. 432–435.
17. Yeo C. I., Jang S. J., Yu J. S., Lee Y. T. 1.3-μm laterally tapered ridge waveguide DFB lasers with second-order Cr surface gratings // IEEE Photonics Technology Letters. – Nov. 2010. – vol. 22, № 22. – pp. 1668–1670.
18. Price R. K., Verma V. B., Elarde V. C., Coleman J. J. Internal loss, modal characteristics, and bend loss of asymmetric cladding ridge waveguide lasers at 850 nm // Journal of Applied Physics. – Jan. 2008. – vol. 103, № 1. – pp. 013108–013108-6.
19. Teng J. H., Lim E. L., Chua S. J., Ang S. S., Chong L. F., Dong J. R., Yin R. Self-aligned metal-contact and passivation technique for submicron ridge waveguide laser fabrication // Journal of Vacuum Science & Technology B: Microelectronics and Nanometer Structures. – Sep. 2008. – vol. 26, № 5. – pp. 1748–1752.
20. Amadjikpe A. L., Papapolymerou J. A high-Q electronically tunable evanescent-mode double-ridged rectangular waveguide resonator // 2008 IEEE Int. Microwave Symp. Dig. – June 2008. – pp. 1019–1022.
21. Serebryannikov A. E., Vasylchenko O. E., Schunemann K. Fast coupled-integral-equations-based analysis of azimuthally corrugated cavities // IEEE Microwave Wireless Comp. Lett. – May 2004. – vol. 14, № 5. – pp. 240–242.
22. Waveguides of complex cross sections / Zargano G. Ph., Lyapin V. P., Mihalevskiy V. S. et al. – Moscow: Radio and Communications, 1986. – 124 p. (in Russian).
23. Jarvis D. A., Rao T. C. Design of double-ridged rectangular waveguide of arbitrary aspect ratio and ridge height // IEE Proc. Microw. Antennas Propagat. – Feb. 2000. – vol. 147, № 1. – pp. 31–34.
24. Rong Y., Zaki K. A. Characteristics of generalized rectangular and circular ridge waveguides // IEEE Trans. Microwave Theory Tech. – Feb. 2000. – vol. 48, № 2.– pp. 258–265.
25. Dubrovka F. F., Piltyay S. I. Electrodynamics boundary problem solution for sectoral coaxial ridged waveguides by integral equation technique // Radioelectronics and Communications Systems. – May 2012. – vol. 55, № 5. – pp. 191–203.
26. Dubrovka F. F., Piltyay S. I. Eigenmodes of sectoral coaxial ridged waveguides // Radioelectronics and Communications Systems. – June 2012. – vol. 55, № 6. – pp. 239–247.

Mittra R., Lee S. W. Analytical Techniques in the Theory of Guided Waves. New York: Macmillan, 191.302 p.

Received in final form December 30, 2013